Improvement of the spatial frequency response of photopolymer materials by modifying polymer chain length

Michael R. Gleeson, Dusan Sabol, Shui Liu, Ciara E. Close, John V. Kelly, and John T. Sheridan*

University College Dublin (UCD) School of Electrical, Electronic and Mechanical Engineering, College of Engineering, Mathematical and Physical Sciences, University College Dublin, Belfield, Dublin 4, Ireland

**Corresponding author: john.sheridan@ucd.ie*

Received August 27, 2007; revised December 10, 2007; accepted January 7, 2008; posted January 9, 2008 (Doc. ID 86926); published February 29, 2008

One of the key predictions of the nonlocal photopolymerization driven diffusion (NPDD) model is that a reduction in the extent of the nonlocal effects within a material will improve the high spatial frequency response. The NPDD model is generalized to more accurately model material absorbtivity. By eliminating the necessity for the steady-state approximation to describe the rate of change of monomer radical concentration, a more accurate physical representation of the initial transient behavior, at the start of grating growth, is achieved, which includes the effects of oxygen-based inhibition. The spatial frequency response of an acrylamide/polyvinylalcohol-based photopolymer is then improved through the addition of a chain transfer agent (CTA), sodium formate. Using the NPDD model demonstrates that the CTA has the effect of decreasing the average length of the polyacrylamide (PA) chains formed, thus reducing the nonlocal response parameter, σ. Further independent confirmation of the resulting reduction in the PA average molecular weight is provided using a diffusion-based holographic technique.

OCIS codes: 090.0090, 090.2900, 090.2890, 160.5470.

1. INTRODUCTION

The storage capabilities of photopolymer materials are under constant study due to their ability to record low loss, highly diffraction efficient volume holographic gratings. These self-processing materials are inexpensive and offer characteristics that make them suitable for commercial use. For practical holographic applications such as data storage, a high spatial frequency material response is necessary, as it is the response to high spatial frequencies that determines the resolution and data storage capabilities.

The nonlocal photopolymerization driven diffusion (NPDD) model has been applied to explain the experimentally observed temporal evolution of holographic grating formation in photopolymers [1–4]. In this paper we examine experimentally and theoretically the spatial frequency response of a simple acrylamide/polyvinylalcohol (AA/PVA) based photopolymer material. Experimental growth curves of unslanted transmission gratings are recorded in our standard AA/PVA material layers for a range of spatial frequencies [1–7]. Theoretically the NPDD model is extended to allow for the dependence of the rate of polymerization on the absorbed illuminating intensity and for inhibition effects. Using our extended NPDD model we then fit the experimentally observed behavior and extract key material parameters. The NPDD model predicts the high-spatial frequency roll-off, observed experimentally, by assuming spatially nonlocal chain growth [5]. A reduction in the polymer chain length will reduce the nonlocality of the polymer chains and hence improve the spatial frequency response of the material. Specifically we aim to achieve this reduction in nonlocal chain growth with the introduction of a chain transfer agent (CTA).

We note that introducing a CTA into the photopolymer material can result in several effects. These include (i) shortening the average length of the polymer chains grown while increasing the number of individual chains; (ii) causing a change in the average, or modulation of, the refractive index in the layers; and (iii) decreasing the rate of diffusion of monomer as a result of a more viscous system. We discuss these issues later in the paper.

The paper is organized as follows. In Section 2, we begin by introducing the process of polymer chain growth in our material, the nonlocal chain length variance, and the effect of this nonlocality. We also present a set of experiments with the aim of validating the process proposed for controlling the length of polymer chains formed. In Section 3, the modified model for a material's response to absorbed intensity is presented [8] along with estimations of our material's absorption parameters. In Section 4, we present the extended NPDD model and the resulting coupled differential equations governing the harmonics of monomer and polymer concentrations. In Section 5, simulations of the behavior of the monomer radical and inhibitor concentrations are presented. In Section 6, the Lorentz–Lorenz relation [9,10] that describes the refractive index of the material layer is presented along with experimental results obtained when it is applied to our material. In Section 7, the experimental procedure for examining the spatial frequency response of the material is explained, and the experimental results obtained are pre-

sented and fit using a four-harmonic numerical fitting algorithm described in Section 4. A comparison of the performance of the standard and the CTA containing material compositions are then presented. A brief conclusion is given in Section 8.

2. POLYACRYLAMIDE CHAIN GROWTH AND DIFFUSION

Our standard dry photopolymer layer typically consists of monomer, binder, cross-linker, an electron donor, and a photoinitiator [1,6]. As the material is exposed to the recording beams the monomer is polymerized, and the amount of polymer formed increases with exposure. When the material is exposed to an interference fringe pattern, more monomer is polymerized in the bright fringes than in the dark fringes. This nonuniform irradiance distribution sets up a spatial monomer concentration gradient and hence results in diffusion of monomer from the dark regions into the bright regions [11,12].

A. Nonlocal Material Response Function

The polymer chains grow away from the point at which they are initiated, and in the adjoining regions the chains continue to remove active monomer. This produces a smeared version of the exposing pattern. If we assume that the chains (molecular weight, length) have a general normal Gaussian probability distribution characteristic [5], then the extent of the nonlocality, that is, the effects of initiation at one point upon polymerization at another, is quantified in the NPDD model by a nonlocal variance parameter, σ. In our NPDD model a nonlocal material response function, $R(x, x'; t, t')$ is used to represent this nonlocal behavior. The nonlocal response function represents the effect of initiation at location x' and t' on the amount of monomer being polymerized at location x and time t [5]. If we assume rapid chain growth compared to other temporal effects, we can neglect the time nonlocality, and the response function reduces to $R(x,x')$ [1], and we assume an action-at-a-distance. The Gaussian spatially nonlocal material response function can be given by

$$R(x,x') = \frac{1}{\sqrt{2\pi\sigma}} \exp\left[\frac{-(x-x')^2}{2\sigma}\right], \tag{1}$$

where σ is the nonlocal response parameter normalized with respect to the grating period [5].

When $\sigma=0$ (local case), the diffusion-based models in the literature explain the existence of a low-frequency cut-off in the spatial frequency response and also the existence of reciprocity failure [5]. However no high-frequency cut-off is predicted to exist. Using the NPDD model, with $\sigma>0$ (nonlocal case), it is found that the larger the nonlocal response variance, the lower the visibility of the profile, but also the more closely the profile recorded resembles the illuminating sinusoidal interference pattern [3,5].

B. Polyacrylamide Chain Length Control

If a controlled reduction of the nonlocal chain-length variance, σ, can be achieved, the potential improvements in the high-spatial frequency material response would be significant. In this paper we aim to achieve this through the addition of a CTA into our simple standard material AA/PVA layers [1,6]. The CTA used in this study is sodium formate (HCOONa), which has a molecular weight of 68.01 g [13–17]. This CTA has the ability to stop the growth of a chain by yielding an atom to the active radical at the end of the growing chain. The CTA is then left as a radical, which can reinitiate the growth of a new chain (depending on the reinitiation efficiency of the CTA [17]), or can be quenched by a terminator or inhibitor. It is proposed that this process will decrease the average length of the polymer chains grown and hence reduce the nonlocal chain-length variance, σ, i.e., localize the chain growth to the bright regions of the interference pattern. Since following termination the CTA can reinitiate chains, we expect the formation of more but shorter polymer chains.

1. Experimental Procedure: Polyacrylamide Diffusion

In order to examine the effects of adding CTA to our AA/PVA material, we first performed a set of simple experiments to measure the effects of the addition of CTA on the rate of decay of the recorded refractive index modulation, Δn, in a resulting holographic grating. By monitoring the rate of decay of holographic gratings, an estimation of the diffusion rate of the polyacrylamide (PA) chains within our material, which will depend on their molecular weight and spatial extent, can be determined. Analyzing a range of material compositions enables the effect of the CTA concentration on the diffusion rate to be observed and allows relevant comparisons to be made. We examine three different materials:

Case 1: standard AA/PVA material composition [1,6].
Case 2: standard material without cross-linker [no bisacrylamide (BA)].
Case 3: standard material without cross-linker and with the addition of CTA.

The cross-linker used in this photopolymer material is BA. This chemical binds the PA chains together, which are formed during the recording process, greatly reducing their mobility. This ensures that the point of chain initiation does not move, otherwise a smearing, through PA diffusion of the recorded fringe pattern, will occur.

Removing or reducing the cross-linker concentration from the material, as in cases 2 and 3 above, has the effect of increasing the mobility of the PA chains. Thus the spatially periodic concentration distribution in the material, formed by the polymer chains, can disperse more rapidly. The resulting increase in the PA rate of diffusion can be observed holographically as a decrease in diffraction efficiency (grating strength) with time [18].

We introduce the CTA into the material in case 3, with the aim of reducing the length of the polymer chains grown. If the CTA works as required and leads to the formation of lower average molecular weight PA chains, there should be an increase in the PA chain mobility, as they will, on average, diffuse more quickly. Therefore, in these experiments we are observing the effect of the diffusion of the PA chains. The diffusion of the PA chains will

reduce the corresponding refractive index modulation and hence a decay in grating strength. This equalization significantly reduces the intensity of the diffracted probe beam.

For each of the three material compositions studied, several growth and decay curves were recorded, using a previously described holographic setup [6,19], involving real time measurement of a diffracted probe beam. This enables (i) the temporal evolution of the grating growth (growth curve) to be monitored; and (ii) the stability or decay of the refractive index modulation, Δn, to be studied during and postexposure. Typical normalized decay curves for the three cases examined can be seen in Fig. 1.

It should be noted that this is a simplified model in which the refractive index variations arise due to the effects of single component constant Fickian diffusion driven decay [20,21]. Any changes in ambient temperature and humidity affect this process, resulting in deviations from the expected ideal exponential decay.

2. Diffusion Model of Grating Decay

The time varying refractive index modulation, $n_1(t)$, can be calculated using Eq. (2), which is derived using Kogelnik's first-order two-wave coupled wave theory [22]:

$$n_1(t) = \frac{\lambda \sin^{-1}\sqrt{\eta(t)}\cos\theta_B}{\pi d}, \tag{2}$$

where λ is the replay wavelength, $\eta(t)$ is the measured time varying diffraction efficiency of the grating, θ_B is the on-Bragg replay angle, and d is the thickness of the grating. As can be seen in Fig. 1 the refractive index modulation in cases 2 and 3 decays more rapidly than in case 1. We describe this decay using the equation

$$n_1(t) = n_1(t \to \infty) + \Delta n_1 \exp[-\alpha_{\mathrm{PA}} t]. \tag{3}$$

The parameters $n_1(t)$ and $n_1(t\to\infty)$ are the time dependent total refractive index modulation and the minimum value of the refractive index modulation, i.e., the value below which the grating will not decay under controlled conditions. The parameter α_{PA} represents the decay constant of the PA chains, which form the grating refractive index modulation, while Δn_1 represents the maximum amplitude of the modulation index variation.

To estimate $n_1(t\to\infty)=n_1(\infty)$ we assume that at some time the diffraction efficiency (η) reaches a constant value, where the η will not fall much lower than this. Therefore, using Eq. (2) we can write that $n_1(t_{\mathrm{final}}) \approx n_1(\infty)$. Manipulating Eq. (3) we can show that

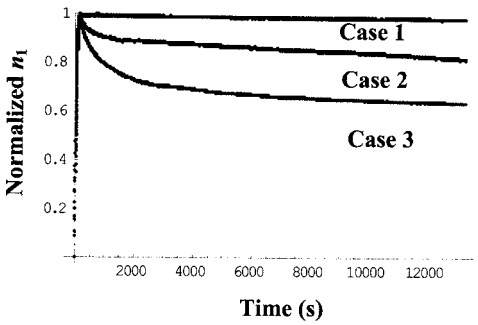

Fig. 1. Postexposure decay curves for cases 1, 2, and 3.

$$\ln[n_1(t) - n_1(t_{\mathrm{final}})] = +\ln[\Delta n_1] - \alpha_{\mathrm{PA}} t. \tag{4}$$

The slope of the line $\ln[n_1(t)-n_1(t_{\mathrm{final}}\sim 12{,}000)]$ as a function of time represents the value of α_{PA}, the rate of decay. We assume that the process governing the decay of the PA distribution is diffusion driven, involving a relaxation of the PA density (concentration) distribution. In practice photopolymerization produces a distribution of the PA molecular weights having a range of diffusion constants. In our analysis we have assumed that there is a single lumped diffusion parameter, D_{PA}. In this case it can be described using Ficks' first law [20,21]. The governing equation, describing the process by which matter is transported from one part of a system to another as a result of random molecular motion, is given by [23]

$$\frac{dC(x,t)}{dt} = D_{\mathrm{PA}}\frac{d^2C(x,t)}{dx^2}, \tag{5}$$

where $C(x,t)$ represents the concentration function in time and position of the polymer chains not cross-linked, i.e., not held rigidly in place, and D_{PA} is the diffusion coefficient of PA chains, which is assumed to be constant throughout the medium. To solve this equation we introduce two other parameters, C_{AV}, the average concentration of polymer chains that are free to diffuse, and C_a, the maximum amplitude of the concentration of the polymer chains that are not held rigidly in place. The solution of Eq. (5) requires the application of two boundary conditions and one initial condition. We assume that when $t=0$

$$C(x,0) = C_{\mathrm{AV}} + C_a\cos[Kx], \tag{6}$$

where $K=2\pi/\Lambda$ is the grating vector magnitude and Λ is the grating period. For this equation to be physical, the concentration function must be positive and finite for all values of x and t, i.e., $0\le C(x,t)\le C_{\mathrm{AV}}+C_a$. Under these conditions the full solution of Eq. (5) is given by

$$C(x,t) = C_{\mathrm{AV}} + C_a\exp\{-D_{PA}K^2t\}\cos[Kx]. \tag{7}$$

Let us assume that the refractive index modulation is linearly proportional to the polymer concentration within the material. Returning to Eq. (3), we expect that

$$\Delta n_1 \exp\{-\alpha_{\mathrm{PA}} t\} \propto C_a \exp\{-D_{\mathrm{PA}}K^2 t\}, \tag{8}$$

implying that

$$\alpha_{\mathrm{PA}} = D_{\mathrm{PA}}K^2. \tag{9}$$

From Eq. (9) it can be seen that the PA diffusion coefficient is linearly related to the decay constant of the grating. This simple model assumes that the diffusion of only one material is responsible for the decrease in diffraction efficiency. In fact both the AA and PA chain concentration distributions will diffuse within the material immediately following exposure [10]. The diffusion constant of the smaller AA molecules would be expected to be much larger, and thus become dispersed much more rapidly than the more bulky PA chains.

By applying the above method to examine the decay curves presented in Fig. 1, estimates for the diffusion rate of the polymer chains were extracted and are presented in Table 1. For case 1, where the standard material contain-

Table 1. Rates of Polymer Diffusion Extracted from Fig. 1 for Cases 1, 2, and 3

	Standard Material Composition	D_{PA} (cm^2/s)
Case 1	0.8 g/100 ml BA	$(7.76\pm4.4)\times10^{-15}$
Case 2	0 g/100 ml BA	$(1.48\pm3.5)\times10^{-14}$
Case 3	0 g/100 ml BA +0.0459 g/100 ml CTA	$(7.32\pm2.1)\times10^{-13}$

ing 0.8 g/100 ml of the BA cross-linker, the diffusion rate was $D_{PA}=(7.76\pm4.4)\times10^{-15}\,cm^2/s$ [24]. For case 2, where the standard material contains no cross-linker (0 g/100 ml), we get $D_{PA}=(1.48\pm3.5)\times10^{-14}\,cm^2/s$. This increase in the diffusion rate in comparison to that estimated in case 1 is to be expected as the mobility of the polymer chains will have increased due to the reduction in the cross-linking of these chains. In case 3 we see a further increase to $D_{PA}=(7.32\pm2.1)\times10^{-13}\,cm^2/s$. There is no BA cross-linker present, which as we have already seen increases PA chain mobility, but more importantly the inclusion of the HCOONa CTA has increased the PA diffusion constant.

Since great care was taken to ensure environmental stability during and between experiments, and since the results obtained are based on averages from reproducible data sets, there appears to be two reasonable explanations for the increase in D_{PA} when CTA is included. It is possible that (i) the addition of the CTA leads to a decrease in the average molecular weight of the PA chains; and/or (ii) the inclusion of the CTA decreases the viscosity of the photosensitive dry layer. If explanation (i) is true then a reduction in the average molecular weight of the PA will in turn reduce the nonlocal chain-length variance, σ. In this case the NPDD model predicts that such a reduction will increase the spatial frequency response of our material. In relation to explanation (ii), in Section 6 we show that the volume fraction of CTA added is very small and has little effect on other bulk material properties, i.e., the average refractive index. In Section 7 we then proceed to demonstrate experimentally an improvement in material spatial frequency response and that the inclusion of the CTA has little effect on the rate of monomer diffusion in the layer.

Before proceeding however we must first extend our existing NPDD model by including the temporal evolution of absorbance in our material and improving the physical representations of inhibition and monomer radical production in the model.

3. ABSORPTION

Previously, the amount of intensity absorbed during grating growth was determined by measuring the amount of light transmitted during exposure and relating it to the incident intensity, corrected for Fresnel and scattering losses [1,4,8,19]. As the molar absorption coefficient and quantum yield of a photosensitizer are major factors in determining the photochemical behavior, it is important to measure and quantify these parameters accurately. By studying the temporal evolution of the medium transmittance [1,4,8,19], estimates for these key material parameters can be found [8]. Thus a general expression can be obtained for the intensity absorbed during exposure for a material whose thickness and initial photosensitizer concentration is known.

Photosensitizer Concentration. Detailed studies of the processes involved during initiation in a photopolymer material have previously been presented in the literature [8,25,26]. When dye molecules are illuminated with an appropriate wavelength, excited state dye molecules are produced, and these excited forms can be converted into radical molecules, which can lead to the initiation of polymer chains or can be returned to their active ground state by processes such as quenching, molecule collisions, radiationless transfer, and inhibition (see Fig. 1 in [1]). If we consider a photopolymer material of thickness d (cm) and photosensitizer concentration A_0 (mol/cm^3), the rate equation for the change in photosensitizer concentration with exposure time can be generated for an incident intensity I_i (mW/cm^2) of known wavelength. The rate equation is given by

$$\frac{dA(t)}{dt} = -\phi I_a(t) + k_r[A_0 - A(t)], \tag{10}$$

where $A(t)$ (mol/cm^3) is the concentration of photosensitizer at time t (s), ϕ (mol/Einstein) is the quantum yield, and k_r (s^{-1}) is the rate of recovery of excited state dye molecules by quenching processes back to its ground state where it is available for further photon absorption. We assume that this recovery effect is negligible over the period of exposure. If the quantum yield and molar absorption are known, $A(t)$ can be predicted using Eq. (10).

To obtain the quantum yield and molar absorption for our material, an expression for the transmitted intensity is generated, and a nonlinear fitting procedure is carried out on experimentally obtained transmission curves [1,8,19]. The absorbed intensity (Einstein/cm^3 s) is given by an adaptation of the Lambert–Beer equation:

$$I_a(t) = I_0'\{1 - \exp[-\varepsilon A(t)d]\}/d, \tag{11}$$

where ε (cm^2/mol) is the molar absorption coefficient. The incident intensity I_i is typically measured in units of mW/cm^2; however, when using Eq. (11) it is necessary to convert this measurement into Einstein/cm^2 s using

$$I_0' = I_i\left(\frac{\lambda}{N_a hc}\right)T_{sf}, \tag{12}$$

which gives the required units for I_0'. In this equation λ (nm) is the wavelength of incident light, N_a (mol^{-1}) is Avogadro's constant, c (m/s) is the speed of light, h (J.s) is Plank's constant, and T_{sf} is an experimentally estimated loss parameter, which takes into account Fresnel and scattered losses. Substituting Eq. (11) into Eq. (10) and integrating with respect to time allows an expression for the photosensitizer concentration to be derived,

$$A(t) = \frac{1}{\varepsilon d} \ln\{1 + [\exp(\varepsilon d A_0) - 1]\exp(-\varepsilon \phi I_0' t)\}. \quad (13)$$

Substituting Eq. (13) back into Eq. (12) yields the time evolution of the absorbed intensity

$$I_a(t) = \frac{I_0'}{d}\left\{\frac{[\exp(\varepsilon d A_0) - 1]\exp(-\varepsilon \phi I_0' t)}{1 + [\exp(\varepsilon d A_0) - 1]\exp(-\varepsilon \phi I_0' t)}\right\}. \quad (14)$$

As previously described [1,8], when light, I_i, is incident on the photopolymer material, the light is either absorbed, I_a, transmitted, I_T, or lost. Equations (12) and (14) can then be related by

$$I_0' = I_a(t) + I_T(t). \quad (15)$$

A transmittance function can also be defined, $T(t) = I_T(t)/I_0$, where I_0 (Einstein/cm^2 s) is the incident intensity before Fresnel correction. Combining these results gives that

$$T(t) = \frac{T_{sf}}{1 + [\exp(\varepsilon d A_0) - 1]\exp(-\varepsilon \phi I_0' t)}. \quad (16)$$

Using an experimental setup similar to that used in [8] we exposed our standard photopolymer material layer [1,6] of thickness d (μm) with initial photosensitizer (erythrosine B) concentration, $A_0 = 1.034 \times 10^{-6}$ mol/cm^3, to a normally incident plane wave of wavelength $\lambda = 532$ nm. During exposure the evolution of the transmitted intensity was carefully monitored. This measurement was then repeated several times under the same conditions with a constant exposure intensity of $I_i = 8$ mW/cm^2 for a range of material thicknesses. From these results, estimations for the molar absorption coefficient, ε, the quantum efficiency, ϕ, and the T_{sf} were then obtained and are presented in Table 2. As can be seen, there is good general agreement for each thickness. The mean value for each parameter is used in the NPDD model calculations presented in Sections 5 and 7.

4. EXTENDED NPDD MODEL

We now present the NPDD model used to study the effects of CTA on our material's spatial frequency response.

A. Previous Analysis

Previously [1–5], it was assumed that during exposure much more monomer is consumed due to polymerization than is consumed in the initiation reaction. This allows an expression for the rate of polymerization, R_p, to be given by

$$R_p \cong -d[M]/dt = k_p[M^\cdot][M], \quad (17)$$

where k_p is the propagation rate constant, $[M]$ is the concentration of monomer, and $[M^\cdot]$ is the concentration of monomer radicals [1]. Furthermore, assuming bimolecular termination and using the rate equations governing the photochemical processes involved during grating formation, a steady-state approximation for the radical concentration was assumed and given by

$$\frac{d[M^\cdot]}{dt} = R_i - 2k_t[M^\cdot]^2 - k_z[Z][M^\cdot] = 0, \quad (18)$$

where R_i is the chain initiation rate, k_t is the rate of termination, $[Z]$ is the concentration of inhibitor, and k_z is the inhibition rate constant [1]. Solving this quadratic equation for $[M^\cdot]$, choosing the physically reasonable root, and substituting this solution into Eq. (17) enabled an expression for the polymerization rate R_p to be generated and expressed as

$$R_p = \frac{k_p[M]}{4k_t}\left\{\sqrt{8k_tR_i + k_z^2[Z]^2} - k_z[Z]\right\}. \quad (19)$$

Initially dissolved oxygen in the material acts as an inhibitor in the polymerization process by reacting with initiating primary radicals formed by electron–proton transfer processes and during the growth of macroradicals, $M_n^\cdot$ [1]. These reactions tend to suppress the creation of monomer radicals and stop polymer chains from starting to form, therefore reducing the rate of polymerization, R_p, and giving rise to an inhibition period, i.e., a dead-band at the start of exposure [1,4,27,28]. Previously we included this process by assuming that during exposure the concentration of inhibitor, $[Z]$, decreased exponentially. In this section, we provide a more complete theoretical basis for the inhibition effects in the NPDD model. In addition, we eliminate the necessity for the use of the steady-state approximation for the rate of change of monomer radical concentration, thus providing a more accurate physical description of the initial transient behavior at the start of grating formation.

Table 2. Parameters Extracted from Fits to Experimentally Obtained Transmission Curves

d (μm)	ε (cm^2/mol) ($\times 10^8$)	ϕ (mol/einstein)	T_{sf}
85	2.014	0.0189	0.792
110	1.941	0.0181	0.800
140	2.220	0.0230	0.680
170	2.041	0.0240	0.678
Mean	**2.054 ± 0.166**	**0.021 ± 0.003**	**0.7375 ± 0.0625**

B. Monomer Radical Concentration

When our photopolymer material is exposed to an interference fringe pattern, the initial concentration of dissolved inhibiting oxygen reacts with the initiating radicals being produced in the bright regions. This nonuniform irradiance causes inhibitor concentration gradients, and hence a diffusion of oxygen from dark regions to bright regions occurs. As the relative size of oxygen molecules are small compared to the surrounding material, it can be assumed that the oxygen is relatively free to move, allowing a one-dimensional (1D) standard diffusion equation for the concentration of inhibitor to be written:

$$\frac{\partial Z(x,t)}{\partial t} = \frac{\partial}{\partial x}\left[D_z(x,t)\frac{\partial Z(x,t)}{\partial x}\right] - k_z Z(x,t)M^{\cdot}(x,t), \quad (20)$$

where $Z(x,t)$ is the inhibitor (oxygen) concentration, $D_z(x,t)$ is the inhibitor diffusion constant, $M^{\cdot}(x,t)$ is the monomer radical concentration, and k_z is the inhibition rate constant [28]. The initial condition is given by $Z(x,0)=Z_0$, for $-\infty<x<\infty$, where Z_0 is the initial concentration of dissolved oxygen. As can be seen in Eq. (20) the inhibitor concentration has a general dependence on the rate of change of monomer radical concentration. In order to solve for the inhibitor concentration, it is therefore necessary to couple Eq. (20) with the rate of change of monomer radical concentration. Rewriting Eq. (18), eliminating the steady-state approximation, gives

$$\frac{\partial M^{\cdot}(x,t)}{\partial t} = R_i - 2k_t[M^{\cdot}(x,t)]^2 - k_z Z(x,t)M^{\cdot}(x,t). \quad (21)$$

If we consider a grating formed by the interference of two plane waves, the spatial distribution of irradiance can be assumed to be cosinusoidal and represented by $I(x)=I_0'[1+V\cos(Kx)]$. As both the rate of change of inhibitor concentration and monomer radical concentration are closely related to the exposure irradiance, their concentrations will be spatially varying periodic even functions of x [2]. The solutions of Eqs. (20) and (21) for Z and $M^{\cdot}$ can therefore be expressed as Fourier series. As the calculation of the Fourier coefficients is algebraically complex, for simplicity during the determination of the monomer radical and inhibitor concentrations, we assume uniform illumination across any local exposed region. Thus the spatial variation is neglected, and Eqs. (20) and (21) reduce to

$$\frac{\partial Z(t)}{\partial t} = -k_z Z(t)M^{\cdot}(t), \quad (22a)$$

$$\frac{\partial M^{\cdot}(t)}{\partial t} = R_i - 2k_t[M^{\cdot}(t)]^2 - k_z Z(t)M^{\cdot}(t). \quad (22b)$$

As in previous studies [1], the rate of initiation R_i is represented by

$$R_i = 2\phi I_a(t), \quad (23)$$

with $\phi=f\phi'$, where ϕ' is the number of radicals produced per light photon absorbed, and it is assumed that due to the cage effect only some fraction f of the free radicals produced react with monomer in the starting reaction [29]. The absorbed intensity, $I_a(t)$, is as described in Eq. (14), and the factor 2 is because monomers are initiated in pairs [17,29].

C. NPDD Model

As before, it is assumed that the polymerization rate $F(x,t)$ is proportional to the exposure irradiance, allowing us to write

$$F(x,t) = F_0(t)[1 + V\cos(Kx)]. \quad (24)$$

As seen in Eq. (17), the polymerization rate is dependent and proportional to the rate of monomer radical generation. If we assume that the polymerization rate constant F_0 is a function of these generated monomer radicals, then

$$F_0(t) = k_p M^{\cdot}(t). \quad (25)$$

This then enables the coupling between the monomer radical and inhibitor concentrations and the temporal changes in absorbed intensity to be incorporated into the general 1D NPDD equation that governs the evolution of the monomer concentration distribution [1–5,10,11].

$$\frac{\partial u(x,t)}{\partial t} = \frac{\partial}{\partial x}\left[D(x,t)\frac{\partial u(x,t)}{\partial x}\right] - \int_{-\infty}^{+\infty}\int_0^t R(x,x';t,t')F(x',t') \times [u(x',t')]^{\beta}dt'dx', \quad (26)$$

where $u(x,t)$ is the free-monomer concentration, $D(x,t)$ is the monomer diffusion constant, and $R(x, x'; t, t')$ is the nonlocal material response function. The diffusion constant is defined by the expression $D(x,t)=D_0\exp[-\alpha F_0(t)t]\cosh[\alpha F_0(t)t]$, where D_0 is the initial diffusion constant and α is the diffusion coefficient's decay parameter [11].

Assuming a bimolecular termination mechanism we derive the NPDD equations when $\beta=1$, where β defines the mode of termination [1,3,10]. In all the analysis and data fitting procedures presented in this paper we assume that the AA and PA concentration distributions can be well described by four-harmonic expansions [1–5]. For brevity we present only the first two coupled differential equations:

$$\frac{du_0(t)}{dt} = -F_0u_0(t) - \frac{1}{2}F_0Vu_1(t), \quad (27a)$$

$$\frac{du_1(t)}{dt} = -S_1F_0Vu_0(t) - [S_1F_0 + D_0K^2 \times \exp(-\alpha F_0t)\cosh(\alpha F_0Vt)]u_1(t) - \left[\frac{S_1}{2}F_0V - D_0K^2\exp(-\alpha F_0t) \times \sinh(\alpha F_0Vt)\right]u_2(t), \quad (27b)$$

where $S_i=\exp(-i^2K^2\sigma/2)$ and u_i are the monomer concentration Fourier harmonic amplitudes. These first-order coupled differential equations are solved numerically with the initial conditions, $u_0(0)=100$ and $u_{m>0}(0)=0$. The concentration of polymerized monomers after an exposure of duration t is given by

$$N(x,t) = \int_0^t\int_{-\infty}^{+\infty} R(x-x')F(x',t')u(x',t')dx'dt', \quad (28)$$

which yields the following polymer concentration spatial-harmonic amplitude:

$$N_1(t) = S\int_0^t F_0\left[Vu_0(t') + u_1(t') + \frac{1}{2}Vu_2(t')\right]dt'. \quad (29)$$

In reality the AA and PA spatial concentration distributions will give rise to a combined refractive index modu-

lation, the temporal evolution of which has previously been studied [10].

5. SIMULATIONS

We now apply this model to characterize our material behavior by experimentally fitting obtained growth curves at different spatial frequencies. In solving Eqs. (21a) and (21b) we describe the variations of the inhibitor and monomer radical concentrations during exposure. Then the solution for the monomer radical concentration can be substituted into Eq. (25) and the variation of the polymerization rate $F_0(t)$ found. Figure 2 was produced by assuming the following typical parameter values: termination rate, $k_t = 5\times10^9$ cm^3/mol s; propagation rate, $k_p = 4\times10^7$ cm^3/mol s; and the initial photosensitizer concentration, $A_0 = 1.034\times10^{-6}$ mol/cm^3. A dry photopolymer layer of thickness $d = 100$ μm was assumed. The mean parameter estimation values from Table 2 for ϕ, ε, and T_{sf} were used in the numerical simulations.

As can be seen in Fig. 2, the inhibitor concentration reduces from an initial dissolved concentration of oxygen, $Z_0 = 1\times10^{-7}$ mol/cm^3 (measured using a dissolved oxygen probe), to zero as it reacts with the monomer radicals produced in the initiation process. The simulation exhibits the same exponentially decaying behavior as was assumed in our previous model [1]. For simplicity inhibitor diffusion, both diffusion inside the volume and diffusion in from the surrounding environment, have been neglected in this analysis. The three curves presented in Fig. 2 are for three different inhibition rates k_z and are presented as follows: solid curve represents $k_z = 1\times10^9$ cm^3/mol s, the large dashed curve represents $k_z = 6\times10^9$ cm^3/mol s, and the small dashed curve represents $k_z = 8\times10^8$ cm^3/mol s. As is expected, the larger the value of the inhibition rate the quicker the inhibitor will be consumed by the radicals.

Figure 3 shows the change in polymerization rate $F_0(t)$, which is proportional to the concentration of monomer radicals produced due to photon absorption. The effect of inhibition can be seen clearly during the initial stages of exposure. Previously we have demonstrated that the dominant mechanism at the start of exposure is inhibition [1]. This effect can be clearly seen in Fig. 3. The reason for this dominant effect is the abundance of inhibitors

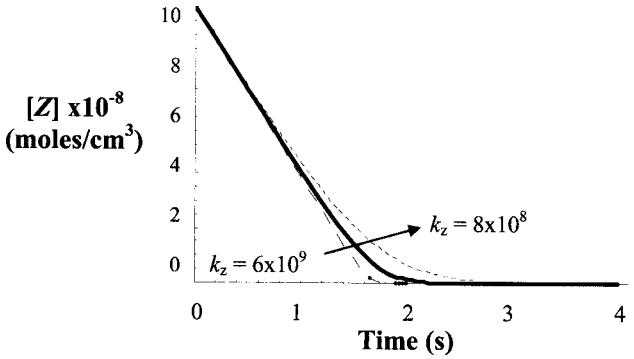

Fig. 2. Simulation of the rate of change of inhibitor concentration with time for three different inhibition rate constants, k_z [cm^3/mol s]: 8×10^8 (small dashed curve); 1×10^9 (solid curve); 6×10^9 (large dashed curve).

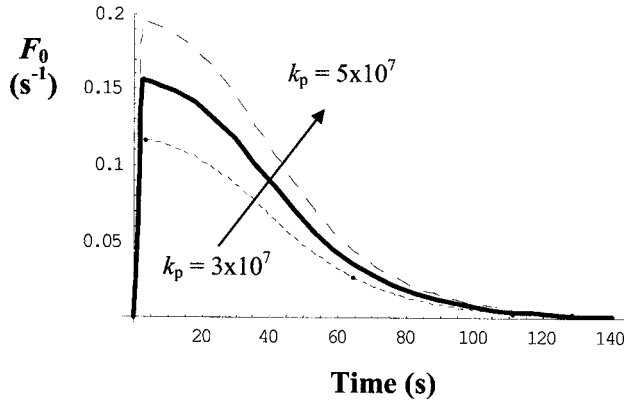

Fig. 3. Simulation of the change in polymerization rate during exposure for three different propagation rates, k_p [cm^3/mol s]: 3×10^7 (small dashed curve); 4×10^7 (solid curve); 5×10^7 (large dashed curve).

(in the form of dissolved oxygen) present at the start of exposure. As the concentration of oxygen decreases, uninhibited polymerization proceeds. Figure 3 shows the polymerization rate simulated for three different rates of propagation, $k_p = \{3\times10^7, 4\times10^7, \text{ and } 5\times10^7\}$cm^3/mol s. As can be seen, an increase in the propagation rate leads to an increase in the rate of polymerization. The figure also shows that the polymerization rate reaches a maximum value and then falls off to zero due to the falloff in absorption and the bleaching of the photosensitizer.

6. AVERAGE REFRACTIVE INDEX

Measurements of the refractive indices of the main components of our photopolymer recording material were carried out. These values are necessary when calculating grating strength (refractive index modulation and diffraction efficiency) and also indicate the impact of the inclusion of CTA on the bulk properties of the material [9,10].

The components of the material are listed in Table 3, the makeup and composition of our material is presented in detail elsewhere [1,6]. Using a Metricon 2010 prism coupler in thick film/bulk material index mode, we measured the refractive indices of the components presented in Table 3. Solutions containing different combinations of material components were prepared and then allowed to dry on glass slides. The refractive indices of the layers were then measured at a wavelength of 633 nm (the wavelength used to probe the grating evolution). The results of these experiments are given in Table 4.

Table 3. Components and Volume Fractions of the Material Makeup

Component	Mass (grams)	Density (g/cm^3)	Volume (cm^3)	Standard Volume Fraction	Volume Fraction with CTA
PVA	7	1.3	5.384615	0.333025	0.32797
AA	2.4	1.122	2.139037	0.132294	0.13028
BA	0.8	1.24	0.645161	0.039902	0.03929
TEA	8.992	1.124	8	0.49478	0.48727
CTA	0.48	1.92	0.25	0	0.01522

Table 4. Measured Refractive Index Values of the Material Components

Material	n^{measured} at $\lambda=633$ nm	$n^{\text{calculated}}$	$n^{\text{literature}}$
PVA	1.5127	1.51270	1.52–1.55[10]
TEA	1.4957	1.48446	1.485 [10]
AA	1.4924	1.47162	1.530 [10]
CTA	1.4941	1.46251	1.4623 [30]
PVA+TEA+AA+BA	1.4951	1.4948	
PVA+TEA+AA+BA+CTA	1.4946	1.4943	

The average refractive index of the material, n, is dependent upon the refractive index of the individual material components and their concentrations or volume fractions. This relationship can be expressed using the Lorentz–Lorenz relation [9,10]:

$$\frac{n^2-1}{n^2+2}=\phi^{(\mathrm{AA})}\frac{n_{\mathrm{AA}}^2-1}{n_{\mathrm{AA}}^2+2}+\phi^{(\mathrm{PVA})}\frac{n_{\mathrm{PVA}}^2-1}{n_{\mathrm{PVA}}^2+2}+\phi^{(\mathrm{BA})}\frac{n_{\mathrm{BA}}^2-1}{n_{\mathrm{BA}}^2+2}+\phi^{(\mathrm{TEA})}\frac{n_{\mathrm{TEA}}^2-1}{n_{\mathrm{TEA}}^2+2}+\left(\phi^{(\mathrm{CTA})}\frac{n_{\mathrm{CTA}}^2-1}{n_{\mathrm{CTA}}^2+2}\right), \tag{30}$$

where n_{AA}, n_{PVA}, n_{BA}, n_{TEA}, and n_{CTA} are the refractive indices of monomer (AA), the binder (PVA), the cross-linker (BA), the electron donor (TEA), and the chain transfer agent (CTA), respectively. $\phi^{(\mathrm{AA})}$, $\phi^{(\mathrm{PVA})}$, $\phi^{(\mathrm{BA})}$, $\phi^{(\mathrm{TEA})}$, and $\phi^{(\mathrm{CTA})}$ are the respective volume fractions of these components where the volume fraction is given by $\phi^{(i)}=x_i v_i/\Sigma x_i v_i$, x_i is the mole fraction, and v_i is the molar volume of the ith component. These volume fractions are presented in Table 3 for both cases, with and without the inclusion of the CTA. We assume that the total volume fraction is approximately conserved during exposure,

$$\phi^{(\mathrm{AA})}+\phi^{(\mathrm{PVA})}+\phi^{(\mathrm{BA})}+\phi^{(\mathrm{TEA})}+\phi^{(\mathrm{CTA})}=1. \tag{31}$$

Combining the data in Tables 3 and 4 and applying the Lorentz–Lorenz relation, the refractive index values for the main components of the material were estimated.

Our measured values of refractive index for PVA and TEA agree closely with those in the literature. Independent verification of our refractive index value for AA is more difficult as it is dependent on the form of the material. However, having used the same method to calculate the refractive index in this case as for the previous components, we believe our result is consistent. The estimated refractive index value for the HCOONa CTA again closely agrees with that in the literature [30]. It can be seen from Table 4 that the measured difference between the materials is in the fourth decimal place, $n=1.4948$ (without CTA) to $n=1.4943$ (with CTA). Furthermore we note that the CTA has the smallest volume fraction contribution listed. All the refractive index values have been estimated based on measurements of dry layers at $\lambda=633$ nm, which replicates the probe conditions.

7. EXPERIMENTAL RESULTS AND PARAMETER ESTIMATION

We now examine the spatial frequency response of (i) standard AA/PVA photopolymer material and (ii) AA/PVA photopolymer material with added HCOONa CTA. We do this by comparing the growth curves and the saturation values of refractive index modulation for a range of spatial frequencies.

For each of the six spatial frequencies examined, several growth curves were recorded with an exposing intensity of $8\ \mathrm{mW/cm^2}$, ($\lambda=532$ nm) using a previously described holographic setup [6,19]. In all cases the diffraction efficiency of a probe beam ($\lambda=633$ nm) was monitored during all of the exposure. An average growth curve and appropriate error bars were identified for each of the spatial frequencies, and the diffracted intensity values, having been corrected for Fresnel reflections, were then converted into grating refractive index modulations using Eq. (2) [22]. The NPDD was then applied to calculate the first harmonic of polymer concentration N_1. For simplicity it is assumed that a linear relationship exists between the recorded refractive index modulation and N_1, i.e., $n_1=C_p N_1$ [3,28]; however, we note that a more complex relationship in fact exists [9,10].

The experimental growth curve data was then fit using the NPDD model predictions. A least squares algorithm in which the mean square error (MSE) between the prediction and the experimental data was minimized is used to obtain the best fit as a function of the material parameters' values. In this way the AA monomer diffusion constant, D_0, the PA propagation rate constant, k_p, termination rate constant, k_t, the refractive index proportionality constant, C_p, and the nonlocal parameter, $S=\exp(-K^2\sigma/2)$, were extracted.

To carry out the fitting process, search ranges of typical parameter values presented in the literature were used [1,5,7,29,31–33]. Values for S were allowed to range from the purely local case, when $S=1$ ($\sigma=0$) to a highly nonlocal case for which $S=0.1$. These S values correspond to a range for $\sqrt{\sigma'}$, the nonlocal response length of $0\leq\sqrt{\sigma'}\leq 345$ nm, where $\sigma=\sigma'/\Lambda^2$. Based on values reported in the literature [31] we might reasonably expect the nonlocal response length to lie in this range.

The mean values obtained for ε, ϕ, and T_{sf} presented in Table 2 were used along with the initial concentrations of photosensitizer and inhibitor, $A_0=1.034\times10^{-6}\ \mathrm{mol/cm^3}$ and $Z_0=1\times10^{-7}\ \mathrm{mol/cm^3}$ for material layers of thickness $d=100\ \mu$m. The rate of inhibition was chosen to be $k_z=1.6\times10^9\ \mathrm{cm^3/mol\ s}$, case 2 in Fig. 2 as it most closely reflected the inhibition behavior in the experimental data. The diffusion decay parameter was chosen arbitrarily to be $\alpha=0.1$, and the exposing fringe visibility was $V=1$.

The parameters estimated from fitting the NPDD model to the experimental growth curves for both materials are presented in Table 5 (standard AA/PVA) and Table 6 (AA/PVA and CTA). For each spatial frequency the saturation refractive index modulation value [n_1^{sat}] is given in the first column of each table.

Examining the parameter estimates for k_p, k_t, and C_p from both tables, it can be seen that they are comparable to one another and to values in the literature [1,5,7,29]. The values obtained for the diffusion constant D_0 lie

Table 5. Spatial Frequency Parameter Estimations for Standard AA/PVA Material Layer

SF (lines/mm) $[n_1^{sat}\times 10^{-3}]$	k_p ($\times 10^7$)	k_t ($\times 10^{10}$)	D_0 ($\times 10^{-11}$)	C_p ($\times 10^{-5}$) cm^3/mol	S	$\sqrt{\sigma'}$ (nm)	MSE ($\times 10^{-10}$)
500 [1.22]	3.20	1.19	2.90	3.72	0.98	64	1.12
1000 [1.81]	4.00	0.84	2.00	4.51	0.94	56	1.41
1500 [1.23]	3.98	0.64	1.50	3.14	0.86	58	0.22
2000 [1.01]	4.18	0.65	0.80	2.81	0.71	66	1.17
2500 [0.74]	3.50	0.72	0.22	2.61	0.59	65	1.15
2750 [0.42]	2.09	1.00	0.95	2.00	0.46	71	0.54
Mean	**3.49±1.4**	**0.86±0.33**	**1.39±1.51**	**3.13±1.38**	—	**63.3±7.7**	**0.93±0.47**

within the search ranges and support the results obtained in our most recent work on diffusion in photopolymers [32]. In particular we note that the mean values for D_0, given in both tables, are similar.

The values obtained for the parameter S have been converted to $\sqrt{\sigma'}$ (nm) values. In Table 5 the mean nonlocal response length in the standard AA/PVA material is estimated to be approximately $\sqrt{\sigma'}\approx 63$ nm. This value agrees with the previous estimates in the literature [3,31]. For AA/PVA with CTA, the corresponding value is $\sqrt{\sigma'}\approx 50$ nm as given in Table 6. This corresponds to a $\sim$20% reduction in the mean $\sqrt{\sigma'}$ value.

Examining the values of the other parameters extracted and presented in Tables 5 and 6 several important points must be made. First, the quality of the numerical fits achieved in all cases are all comparably good with MSE values of $\sim 10^{-10}$. Second, following an exhaustive and independent search procedure the mean values of all the other parameters estimated remained similar while only the nonlocal parameter varied significantly. Returning to Section 2 we recall that one possible cause of our observed increased rate of diffusion of PA with the inclusion of CTA was a change in average material viscosity. Among those parameters estimated in Tables 5 and 6 is the monomer diffusion constant, D_0. Since it is not found to change appreciably, we believe only a shortening of the PA chains consistently explains the resulting improvement in spatial frequency response.

To more clearly illustrate this improvement in material performance and to demonstrate the quality of our numerical fits to the data, the results used to produce the row of parameter values in Tables 5 and 6 for the 2750 lines/mm spatial frequency case are shown in Fig. 4. The data presented and the associated error bars results from five to ten repetitions of the same exposure in identically produced and exposed dry layers. For this particular concentration and type of CTA an average improvement of $\sim$17% in the refractive index modulation is observed. It can also be seen that there is a negligible difference in the rate of polymerization in both growth curves presented. This implies an efficient reinitiation of chains is taking place [29], which is consistent with our result that a larger quantity of PA chains of smaller molecular weight (i.e., shorter length) are formed.

8. CONCLUSIONS

The NPDD model was generalized to more closely model material behavior during grating formation. An expression for the change in the absorbed intensity during exposure is presented and the key material parameters controlling the absorption characteristics are estimated. By eliminating the necessity for the steady-state approximation, a more physical representation of the rate of change of monomer radical concentration and hence, the initial transient behavior, is achieved. Thus a time-varying change in the polymerization rate has been included in the NPDD model.

The spatial frequency response of an AA/PVA photopolymer has been improved through the addition of a CTA, HCOONa. The link between this improvement and the effects of the CTA has been confirmed on the basis of experimental results using a diffusion-based holographic technique and through the estimation of material parameters using the extended NPDD model. The CTA has the effect of decreasing the average length of the PA chains

Table 6. Parameter Estimations for Spatial Frequencies in AA/PVA and CTA Material

SF (lines/mm) $[n_1^{sat}\times 10^{-3}]$	k_p ($\times 10^7$)	k_t ($\times 10^{10}$)	D_0 ($\times 10^{-11}$)	C_p ($\times 10^{-5}$)	S	$\sqrt{\sigma'}$ (nm)	MSE ($\times 10^{-10}$)
500 [1.22]	3.20	1.39	2.90	3.66	0.99	45	0.49
1000 [1.85]	4.00	1.14	1.90	4.50	0.94	55	1.32
1500 [1.23]	3.51	0.66	0.81	3.37	0.92	43	1.71
2000 [1.17]	4.00	0.60	0.62	3.13	0.82	50	1.46
2500 [0.77]	4.06	0.67	0.51	2.10	0.73	50	1.85
2750 [0.50]	3.01	1.20	1.10	1.13	0.63	55	1.22
Mean	**3.63±0.6**	**0.94±0.45**	**1.33±1.5**	**2.98±1.8**	—	**49.6±6.6**	**1.34±0.85**

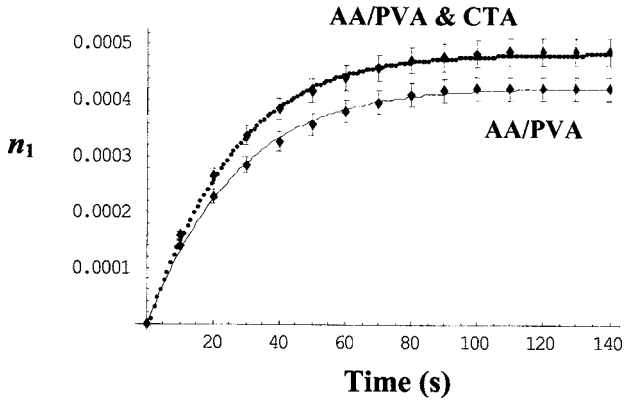

Fig. 4. Experimental growth curve data and fits at 2750 lines/mm. Standard material (solid curve); with CTA (dashed curve).

formed. The chain transfer kinetic effects [17,29] introduced by the CTA, which may contribute to the increased localization of the polymerization, may include: (a) an increase in the concentration of the monomer radicals available for bimolecular termination, and/or (b) the effects of less than 100% efficiency in the reinitiation process. These effects result in a reduction in the nonlocal parameter, from 63 to 50 nm. Given that a carbon–carbon (C–C) bond is approximately 0.15 nm long and an carbon atom is ~0.1 nm long, a PA repeat unit of length 0.5 nm would not be unexpected. Given that coiled polymer chains may contain from hundreds to tens of thousands of repeat units, the lengths predicted by this model seem physically reasonable.

Thus, in this paper, the prediction of the NPDD model that a reduction in the extent of the nonlocal effects within a material will improve the high-spatial frequency response, has been confirmed. The NPDD model presented in this paper suffers from several serious deficiencies that limit the accuracy of the results. The discussion neglects all three-dimensional effects [33], i.e., variations with depth, and a more exact expression for the refractive index modulation calculated using the Lorentz–Lorenz equation must be applied [10]. Furthermore, to avoid numerical difficulties, fully rigorous finite time domain analysis should be used [10]. Other effects such as the choice of the dominant chain termination mechanisms [3], multicomponent diffusion, and shrinkage effects must also be included.

Experimentally a range of CTAs and concentrations are currently being examined so as to better understand the chain transfer kinetics taking place in our photopolymer material. Full analysis and examination of this kinetic behavior, such as the rate of chain transfer (Gregg and Mayo method [14,29]), the reinitiation rate and the reinitiation efficiency are crucial to enable further control of chain locality. This study may eventually allow a clearer link between the nonlocal variance metric and the PA molecular weight to be found.

ACKNOWLEDGMENTS

We acknowledge the support of Enterprise Ireland and Science Foundation Ireland through the Research Innovation, the Proof of Concept Funds, and the Basic Research and Research Frontiers Programs. We also thank the Irish Research Council for Science, Engineering, and Technology and SPIE through the SPIE Educational Scholarship.

REFERENCES

1. M. R. Gleeson, J. V. Kelly, and J. T. Sheridan, "Modelling the photochemical effects present during holographic grating formation in photopolymer materials," J. Appl. Phys. **102**, 1–9 (2007).
2. J. R. Lawrence, F. T. O'Neill, and J. T. Sheridan, "Adjusted intensity non-local diffusion model of photopolymer grating formation," J. Opt. Soc. Am. B **19**, 621–624 (2002).
3. J. V. Kelly, F. T. O'Neill, and J. T. Sheridan, "Holographic photopolymer materials: non-local polymerization driven diffusion under non-ideal kinetic conditions," J. Opt. Soc. Am. B **22**, 407–416 (2005).
4. M. R. Gleeson, J. V. Kelly, C. E. Close, F. T. O'Neill, and J. T. Sheridan, "The effects of absorption and inhibition during grating formation in photopolymer materials," J. Opt. Soc. Am. B **23**, 2079–2088 (2006).
5. J. T. Sheridan and J. R. Lawrence, "Non-local response diffusion model of holographic recording in photopolymer," J. Opt. Soc. Am. A **17**, 1108–1114 (2000).
6. J. R. Lawrence, F. T. O'Neill, and J. T. Sheridan, "Photopolymer holographic recording material," Optik (Stuttgart) **112**, 449–463 (2001).
7. F. T. O'Neill, J. R. Lawrence, and J. T. Sheridan, "Comparison of holographic photopolymer materials by use of analytic non-local diffusion models," Appl. Opt. **41**, 845–852 (2002).
8. L. Carretero, S. Blaya, R. Mallavia, R. Madrigal, A. Belendez, and A. Fimia, "Theoretical and experimental study of the bleaching of a dye in a film-polymerization process," Appl. Opt. **37**, 4496–4499 (1998).
9. I. Aubrecht, M. Miller, and I. Koudela, "Recording of holographic gratings in photopolymers: theoretical modelling and real-time monitoring of grating growth," J. Mod. Opt. **45**, 1465–1477 (1998).
10. J. V. Kelly, M. R. Gleeson, J. T. Sheridan, S. Gallego, and C. Neipp, "Temporal analysis of grating formation in photopolymer using the non-local polymer driven diffusion model," Opt. Express **13**, 6990–7004 (2005).
11. G. Zhao and P. Mouroulis, "Diffusion model of hologram formation in dry photopolymer materials," J. Mod. Opt. **41**, 1929–1939 (1994).
12. S. Piazolla and B. K. Jenkins, "First-harmonic diffusion model for holographic grating formation in photopolymers," J. Opt. Soc. Am. B **17**, 1147–1157 (2000).
13. M. Pabon, J. Selb, F. Candau, and R. G. Gilbert, "Polymerization of acrlyamide in solution and inverse emulsion: number molecular weight distribution with chain transfer agent," Polymer **40**, 3101–3106 (1999).
14. M. Fevola, R. Hester, and C. McCormack, "Molecular weight control of polyacyrlamide with sodium formate as a chain-transfer agent: characterization via size exclusion chromatography/multi-angle laser light scattering and determination of chain-transfer constant," J. Polym. Sci., Part A: Polym. Chem. **41**, 560–568 (2003).
15. L. A. Goretta and R. R. Otremba, Formic acid alkali metal formates as chain transfer agents in the preparation of acrylamide polymers, U.S. patent 4,307,215 (December 22, 1981).
16. H. A. Gartner, Process for the production of high molecular weight copolymers of diallyammonium monomers and acrylamide monomers in an aqueous dispersed phase, U.S. patent 5,171,783 (December 15, 1992).
17. M. C. Cole, F. R. Askham, and W. L. Wilson, "Holographic recording medium with control of photopolymerization and dark reaction," U.S. patent 2006/0194120 A1 (August 31, 2006).
18. F. T. O'Neill, J. R. Lawrence, and J. T. Sheridan,

"Improvement of holographic recording material using aerosol sealant," J. Opt. A, Pure Appl. Opt. **3**, 20–25 (2001).
19. M. R. Gleeson, J. V. Kelly, F. T. O'Neill, and J. T. Sheridan, "Recording beam modulation during grating formation," Appl. Opt. **44**, 5475–5482 (2005).
20. P. W. Atkins, *Physical Chemistry*, 4th ed. (Oxford U. Press, 1992).
21. J. Crank, *The Mathematics of Diffusion*, 2nd ed. (Oxford U. Press, 1975).
22. H. Kogelnik, "Coupled wave theory for thick holographic gratings," Bell Syst. Tech. J. **48**, 2909–2947 (1969).
23. J. Crank and G. S. Park, *Diffusion in Polymers*, 1st ed. (Academic, 1968).
24. S. Gallego, M. Ortuno, C. Niepp, A. Marquez, A. Belendez, and I. Pascual, "Characterization of polyvinyl alcohol/acrylamide holographic memories with a first-harmonic diffusion model," Appl. Opt. **44**, 6205–6210 (2005).
25. D. J. Lougnot and C. Turk, "Photopolymers for holographic recording: II. Self-developing materials for real-time interferometry," Pure Appl. Opt. **1**, 251–268 (1992).
26. D. J. Lougnot and C. Turk, "Photopolymers for holographic recording: III. Time modulated illumination and thermal post-effect," Pure Appl. Opt. **1**, 269–279 (1992).
27. A. Fimia, N. Lopez, F. Mateos, R. Sastre, J. Pineda, and F. Amat-Guerri, "Elimination of oxygen inhibition in photopolymer systems used as holographic recording materials," J. Mod. Opt. **40**, 699–706 (1993).
28. A. K. O'Brien and C. N. Bowman, "Modelling the effect of oxygen on photopolymerization kinetics," Macromol. Theory Simul. **15**, 176–182 (2006).
29. G. Odian, *Principles of Polymerization* (Wiley, 1991).
30. H. Inaba and H. Naito, "Measurement of the refractive indices of lithium-sodium formate and sodium formate crystals," Opto-electronics (London) **5**, 551–555 (1973).
31. S. Wu and E. N. Glytsis, "Holographic grating formation in photopolymers: analysis and experimental results based on a nonlocal diffusion model and rigorous coupled-wave analysis," J. Opt. Soc. Am. B **20**, 1177–1188 (2003).
32. C. E. Close, M. R. Gleeson, F. T. O'Neill, J. V. Kelly, and J. T. Sheridan, "Control and measurement of the physical properties in acrylamide based photopolymer materials," Proc. SPIE **5827**, 346–357 (2005).
33. S. Gallego, M. Ortuno, C. Niepp, A. Marquez, A. Belendez, J. V. Kelly, and J. T. Sheridan, "3 Dimensional analysis of holographic photopolymers based memories," Opt. Express **13**, 3543–3557 (2005).